Received: 7 April 2021 | Revised: 25 August 2021 | Accepted: 29 August 2021

DOI: 10.1002/eng2.12459

RESEARCH ARTICLE

Engineering Reports Open Access WILEY

Impact of processing parameters in plasma electrolytic oxidation on corrosion resistance of magnesium alloy type AZ91

Talal A. Aljohani[1] | **Sami Aljadaan**[1] | **Meteb T. Bin Rubayan**[1] | **Fuad Khoshnaw**[2]

[1]National Centre for Corrosion Technology, King Abdulaziz City for Science and Technology, KACST, Riyadh, Saudi Arabia

[2]School of Engineering and Sustainable Development, De Montfort University, Leicester, UK

Correspondence
Talal A. Aljohani, National Centre for Corrosion Technology, King Abdulaziz City for Science and Technology, KACST, Riyadh, Saudi Arabia.
Email: taljohani@kacst.edu.sa

Funding information
De Montfort University; King Abdulaziz City for Science and Technology, Grant/Award Number: (Ref. no. 37502500)

Abstract

This study aims to investigate the effect of the processing parameters in plasma electrolytic oxidation (PEO) on the corrosion resistance of magnesium alloy type AZ91. The PEO coatings were prepared on the samples using alkaline-based electrolyte. Both unipolar and bipolar, different frequencies and duty cycles were applied. Corrosion tests, using potentiodynamic polarization, linear and cyclic, and electrochemical impedance spectroscopy techniques, were applied on the as-received and PEO coated samples. Scanning electron microscopy was used to investigate the surface morphology, for example, micropores, as well as to measure the thickness of the coated layer by changing the processing parameters. The results show that the size of micropores is interrelated to the duty cycle percentage and current polarities, as the higher frequency causes thinner coating layers, with fewer micropores, consequently higher corrosion resistance. In addition, increasing the duty cycle, a denser and more compact coating was obtained. The XRD results showed a missing peak of the α-Mg phase in a PEO coated sample using bipolar, the highest frequency (1666 Hz), and the highest duty cycle (66.6%). The mils per year calculations showed that the PEO coated has a lower corrosion rate by at least 8 times than the as-received alloy.

KEYWORDS

AZ91, electrochemical impedance spectroscopy, plasma electrolytic oxidation, potentiodynamic polarization

JEL CLASSIFICATION

Materials science

1 | INTRODUCTION

The features such as high strength/weight ratio, good machinability, thermal conductivity, and electromagnetic shielding make the magnesium alloys highly used in different industries such as automobile, aerospace, and electronics industries.[1–5] Magnesium alloys, also, are used in clinical applications such as biodegradable implants for

cardiovascular, musculoskeletal, and general surgery.[6,7] However, due to its high reactivity, magnesium has low corrosion resistance and the oxide film on its surface easily can break.[8] Therefore, researchers are continuously attempting to improve the performance of magnesium alloys in various fields.

Anodizing, where aluminium is coated on magnesium, is among the traditional methods, which has been used for a while, to improve the corrosion resistance, however, because the mechanical properties of aluminium are relatively low, for example, yield strength, hence, other attempts have been conducted, such as adding nanoparticles and forming a hybrid coating, using plasma electrolyte oxidation (PEO).[9–18]

PEO electrolytic plasma oxidation (EPO), which is also known as MAO, is an electrochemical surface treatment process for generating oxide coatings on metals. This process is similar to the anodizing, but with applying higher potentials. In general, the process depends on the modification of a conventional anodically grown oxide film through applying an electric field much greater than the dielectric breakdown field of the oxide. Therefore, during discharging, the resulting plasma-chemical reactions contribute to the growth of the coating. Coating properties depend on the substrate alloy, the electrolyte, and electrical parameters.[1–4,19–21]

The mechanism of the PEO coatings on magnesium alloys has been investigated by applying electrochemical measurement, and optical spectroscopy and acoustic emission spectrometer. The performance of the coatings has been characterized by measuring the wear and corrosion rates. Besides, the biocompatibility tests of PEO coatings have been considered.[22]

Francis et al.[16] studied the pre-treatment of magnesium alloy type AZ91 in alkaline silicate solution by anodic oxidation in the presence of sodium salicylate. The electrochemical corrosion behavior of anodized films was investigated using electrochemical impedance spectroscopy (EIS). The results showed a significant increase in corrosion resistance. Liang et al.[17] worked on two types of PEO coatings on AM50 magnesium alloy using pulsed DC plasma electrolytic oxidation process in an alkaline phosphate and acidic fluorozirconate electrolytes. The corrosion behavior of the coated samples was evaluated by electrochemical techniques in neutral 0.1 M NaCl solution. The results showed that the PEO coating which was composed of only MgO suffered from localized corrosion, whereas the PEO coating with ZrO_2 compounds showed higher stability and provided efficient corrosion protection. Lu et al.[18] used PEO with nano-and micro-sized SiO_2 particles to seal the porosity, then tested at different KOH concentrations. Yang et al.[23] used PEO to improve the corrosion resistance and biocompatibility of porous MgO-CaP coatings by adding hydroxyapatite (HA) particles. The results showed that most HA particles were reactively incorporated into the PEO coatings and the coating microstructure was significantly modified with increasing the concentration of HA, which resulted in higher corrosion resistance. Hussein et al.[24] studied the PEO mechanism by investigating the formation of a coating layer, up to 110 μm thickness on AJ62 Mg alloy. They found that during the PEO process some of the metal cations are transferred outwards from the substrate and react with anions to form ceramic coatings. At the same time, due to the high electric field in the discharge channels, oxygen anions transfer toward the magnesium substrate and react with Mg^{+2} cations to form a ceramic coating. Lu et al.[25] studied the influence of SiO_2 particles on the microstructure, phase composition, corrosion, and wear performance of PEO coatings on AM50 Mg alloy. Different electrolyte compositions were applied to fabricate coatings in an alkaline, phosphate-based electrolyte, aiming to control the incorporated amount of the particles in the layer. It was found that the uptake of particles was accompanied by the coating growth at the initial stage, while the particle content remained unchanged at the final stage, which is dissimilar to the evolution of the coating thickness. They found that the corrosion performance of the coating mainly depends on the barrier property of the inner layer, while wear resistance primarily relies on the coating thickness.[25,26]

Pezzato et al.[27] used nanoindentation, potentiodynamic polarization (PDP), EIS and scanning vibrating electrode tests to evaluate the mechanical properties and the corrosion resistance of PEO-coated AZ80 magnesium alloy before and after a sealing treatment in boiling water. The samples were produced in a solution containing silicates and phosphates and working at high current densities with short treatment times. The results showed that the sealing did not influence the microstructure and the mechanical properties of the samples and instead produced a remarkable increase in the corrosion resistance. The crevice corrosion, present in the sample without the sealing, was avoided with the treatment in boiling water.

Cao et al.[28] studied PEO process with an alkaline borate solution—contained organic additive without F, P, and Cr—on Mg-based alloy type AZ91D alloy using 50 Hz AC anodizing technique, through applying different anodizing parameters. It was found that the formation of the anodic films was always coupled with sparking and oxygen evolution, whose intensity changed with the additive and anodizing voltage. However, the addition of an organic additive, to seal the pores, showed no significant effect on corrosion resistance.

Sreekanth et al.[26] developed PEO coatings on AZ31 magnesium alloy using alkaline silicate with KOH as a base electrolyte system, adding different sodium aluminate, sodium tetra-borate, potassium titanium fluoride, trisodium ortho-phosphate, and urea as additives. The results showed that the sample treated by PEO in the electrolyte solution, containing sodium tetra-borate as an additive, showed higher corrosion resistance.

Ghasemi et al.[29] used four different electrolytes including either potassium or sodium hydroxides. Electrolyte conductivity and breakdown voltage were measured to correlate the property of the coating to the type of the electrolyte. The EIS results indicated the presence of porous and compact layers in the structure of the PEO coatings. While the corrosion resistance was mainly attributed to the compact layer, the role of the porous layer, as a barrier, against corrosion was negligible.

Duan et al.[30] described the growth process of the oxide film formed on magnesium alloy AZ91D under PEO in an alkaline silicate solution. It was found that at the initial stage (before the occurrence of sparking), the growth rate of PEO films is low, the elements (O, Mg, Al, and Si) contents were varied, and the donor concentration in the film was kept at a high level. However, after sparking, the PEO films showed a higher growth rate. On the other hand, the results showed that with increasing the treated time, the thickness of PEO films and transfer resistance to ions and electrons were also increased; thereby, the growth rate of the PEO films was decreased.

Due to the complexity of the formation of PEO coatings, there are still some factors requiring in-depth studies. To fill this gap, this research has examined the impact of using unipolar and bipolar currents on PEO coating of AZ91 alloy.

2 | MATERIALS AND EXPERIMENTAL WORKS

Magnesium alloy type AZ91 was used in this study, the chemical composition in wt%—as it is provided by Neo-Cast, is 9.04 Al, 0.695 Zn, 0.28 Mn, 0.0026 Fe, 0.00107 Be, 0.031 Si, 0.0013 Cu, and Mg balance. Samples were cut into rectangular shapes with dimensions equal to $11 \times 4.5 \times 1$ cm the sample area was fixed as 130 cm^2. No pre-treatments were applied to the samples before the plasma electrolytic process. The PEO process was performed via a MARIS GS 150 DC plasma power supplies purchased from ADL GmbH, in a polyvinyl chloride container (PVC) lined with a 1 m^2 stainless-steel sheet which was used as a counter electrode, while the specimen was acting as the working electrode. The PEO was carried out in an alkaline solution comprising 3 g/L of potassium hydroxide [KOH]. The whole system was connected to a cooling system to keep the temperature around 25°C and the solution was kept mixed using air agitation. For safety measures, the whole system was placed inside a fume hood.

To investigate the effect of polarity of the process on the coating layer structure and its thickness, both unipolar and bipolar methods were applied, using different frequency and duty cycles. The experiment duration was 300 s. Table 1 describes the PEO electrical conditions that were applied. Duty cycle percentage for working electrode was calculated based on the following equation:

$$\text{duty cycle} = \frac{t_{on}}{t_{on} + t_{off}} \tag{1}$$

where t_{on} is on time, t_{off} is off time, and $(t_{on} + t_{off})$ is the whole time.

TABLE 1 The applied parameters; frequencies, currents, and coating thickness

Samples	Polarity	Frequency (Hz)	Off/on (ms)	Duty cycle %	Working electrode (mA/cm^{-2})		Ave. coating thickness (μm)
AZ91-PEO 1	Unipolar	1000	0.7/0.3	30	+0.23	0	17
AZ91-PEO 2	Bipolar	1000	0.7/0.3	30	+0.23	−0.08	12
AZ91-PEO 3	Bipolar	1666	0.2/0.4	66.6	+0.23	−0.08	6
AZ91-PEO 4	Bipolar	1000	0.5/0.5	50	+0.23	−0.08	8

3 | ELECTROCHEMICAL TESTS AND CHARACTERIZATION

A Potentiostat type Bio-Logic SP-200 and flat corrosion cell—with three electrodes—were used, to perform the electrochemical corrosion tests. The platinum and saturated calomel electrodes were used as counter and reference electrodes respectively. The potential scan rate for the polarization technique was 0.166 mV s^{-1} to ensure a steady-state condition. A linear polarization scan was applied in a short potential range of ±25 mV. The EIS tests were performed at the open-circuit potential, $E_{corr,}$ by applying a sinusoidal voltage between ±10 mV within a frequency range of 10 mHz to 100 kHz. The electrochemical measurements were performed at aerated 0.5 M sodium chloride at 298 K.

The surface morphology of the corroded samples was investigated using a scanning electron microscope (SEM) type JSM-IT300 InTouchScope™ in combination with an X-MaxN Oxford energy-dispersive X-ray spectroscopy (EDS) analyzer. The crystallinity of the structure was explored using X-ray diffraction type JEOL JDX-8030 X-ray diffractometer with Cu Kα radiation operating at 40 kV and 30 mA at a scan rate of 2°/min.

4 | RESULTS AND DISCUSSION

4.1 | Surface morphology

Figure 1 shows SEM images of the Mg samples coated by PEO before and after corrosion tests. Figure 2A,B show the as-received AZ91 alloy before and after applying the corrosion test respectively. The coated samples showed micro-holes, with different sizes and shapes, which were evolved by applying different frequency and duty cycle percentage.

Figure 1C shows large holes for the coated sample processed with 30 mA, unipolar- PEO 1, while Figure 1E smaller pores sizes (but with more numbers) for the sample prepared with PEO 2 parameters—with using the same coating parameters, bipolar, moreover Figure 1I shows even much less. On the other hand, Figure 1G shows a mix pattern of large and small holes, for the sample prepared for PEO 4, with increasing the duty cycle, bipolar, and equal on/off time. On the other hand, that the pores sizes were smaller for the sample prepared with PEO 3 parameters—by reducing the processing time and increasing the frequency. This agrees with Gh. Barati et al.[22] results, their study found that pore size is a function of the discharge density and processing time. The coated samples, as shown in Figure 1D,F,H,J, however, show no significant corrosion except the surface was slightly darkened.

Figure 2 shows the SEM and EDX results of as-received alloy AZ91 after electrochemical corrosion test. The basic microstructure of AZ91 magnesium alloy consists of primary α-phase in which aluminium rich β-phase, light phases (see Figure 2A) is precipitated along the grain boundaries. Large pits, as shown as dark areas, are shown in the figure, which represents severe corrosion compared to coated samples presented in Figure 1B,D,F,H,J. In addition, the EDS analysis (as shown in Figure 2B) displays corrosion products where Mg content reduced significantly.

Figure 3 shows that the coating thickness for samples prepared at low frequency that is, 1000 Hz ranges around 14 μm. The thickness significantly decreased by increasing frequency to 1666 Hz, see Table 1, which indicates that both the thickness and pores size are affected by frequency. The images show similar thicknesses between samples coated under similar frequencies but with different polarities, PEO-1 and 2. Moreover increasing duty cycle reduce the thickness significantly as exhibited by the samples PEO -3 and 4.

4.2 | Composition

Figure 4 shows XRD patterns that refer to the appearance of the related elements. The indices indicate the composition of Mg, MgO, $MgAl_2O_4$, and $Mg_{17}Al_{12}$. The layered result is constituted mainly by Mg and MgO due to the composition of the alloy and the electrolyte while the other elements due to the reflection of the alloy. Comparing the peaks of the PEO sample with the as-received AZ91 sample shows slight changes in the intensity of the compositions that can be attributed to the changes in the coating parameters, for example, lower and higher peaks were for the as-received AZ91

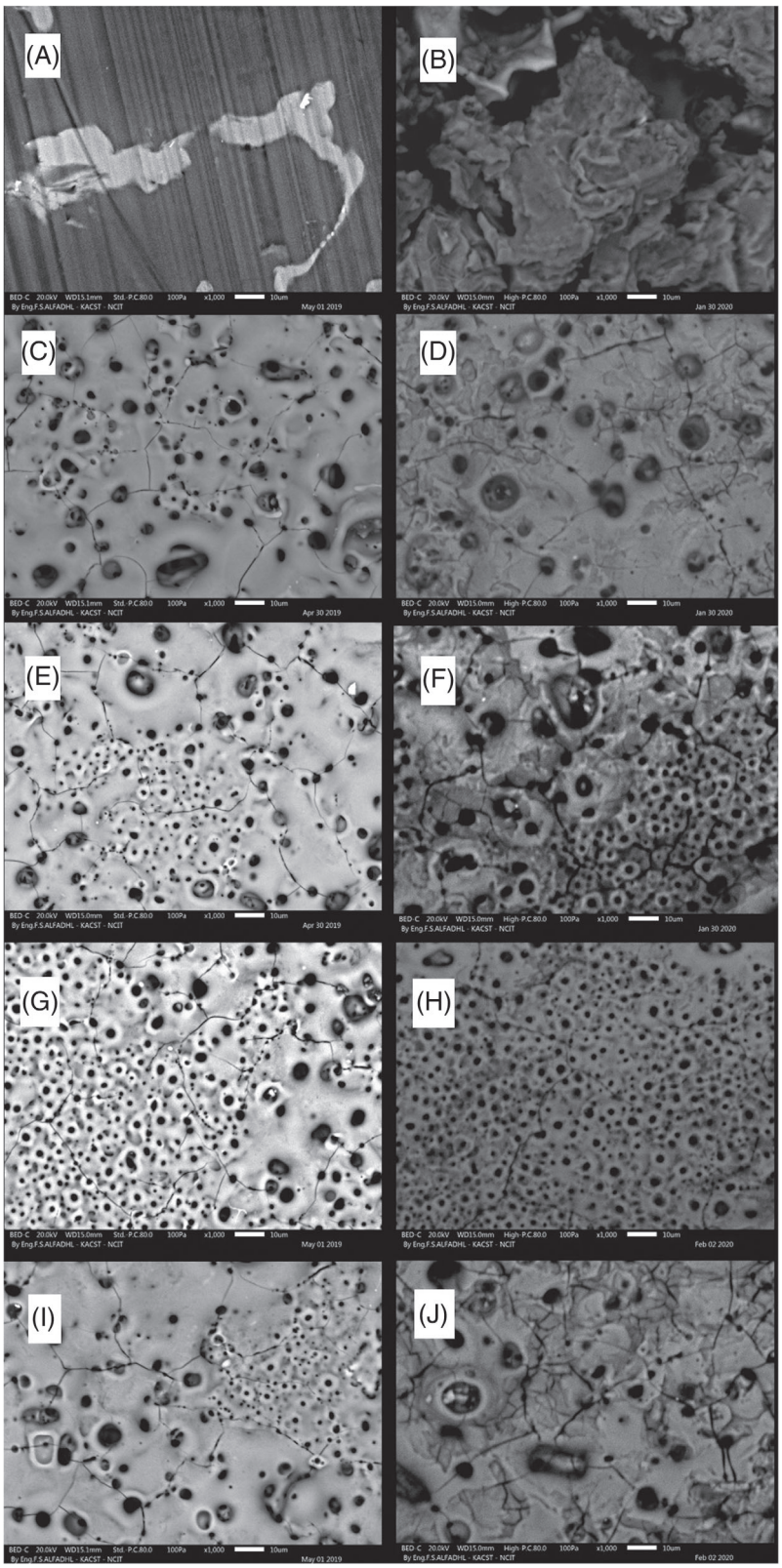

FIGURE 1 Surface morphologies before (left) and after (right) corrosion test: pure AZ91 (A, B), AZ91-PEO 1 (C, D), AZ91-PEO 2 (E, F), AZ91-PEO 3 (G, H) and AZ91-PEO 4 (I, J)

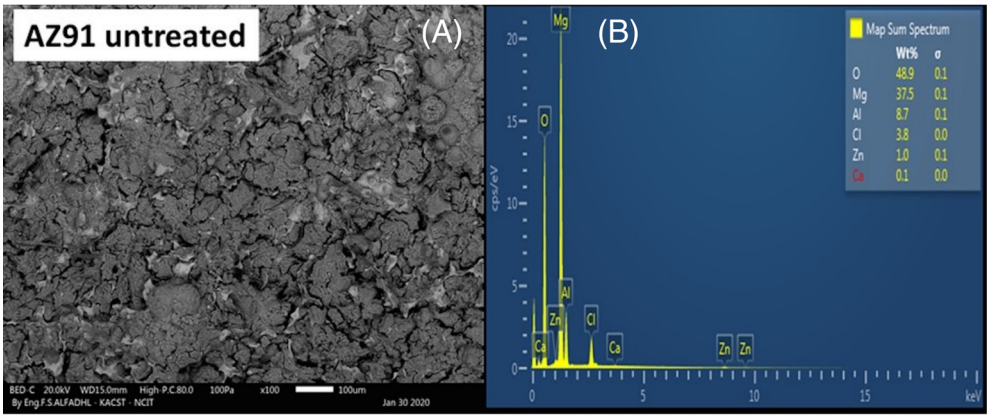

FIGURE 2 SEM images (A) and EDS analysis (B) of as-received AZ91 after corrosion test examined in aerated 0.5 M sodium chloride at 298 K

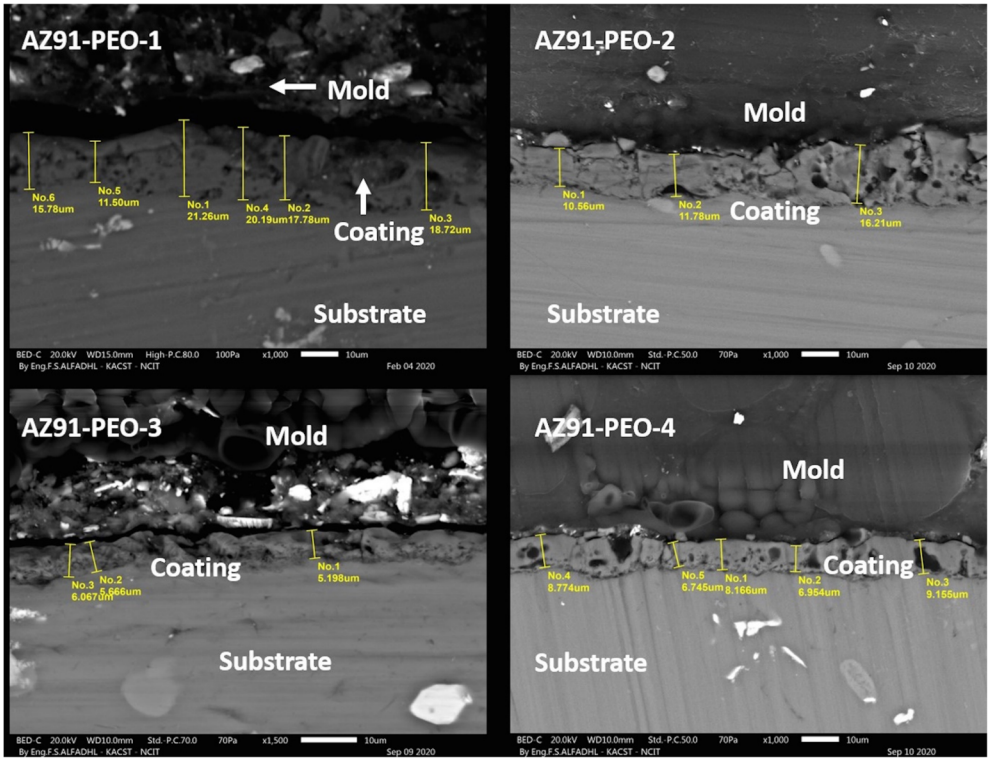

FIGURE 3 Cross-section images of samples with different PEO coatings parameters

and AZ91-PEO-4, respectively. In addition, the PEO-3 shows a different pattern compared with the others, in terms of light spots, which can be either $Mg_{17}Al_{12}$ or MgO beads.

Figure 5A shows the XRD patterns of the samples after electrochemical corrosion tests. The peak intensity for as-received AZ91 significantly increased after its exposure to corrosion, while the opposite is true for the PEO coated samples, as the peak intensity decreased. Besides, the as-received AZ91 and all the PEO coated samples, except the AZ91-PEO-3, display an extra peak at = 34.7° which is associated with α-Mg.[31] Figures 1 and 3 showed that the PEO-3 had a distinct surface morphology and thickness with smaller micropores and more compacted coatings, as mentioned above.

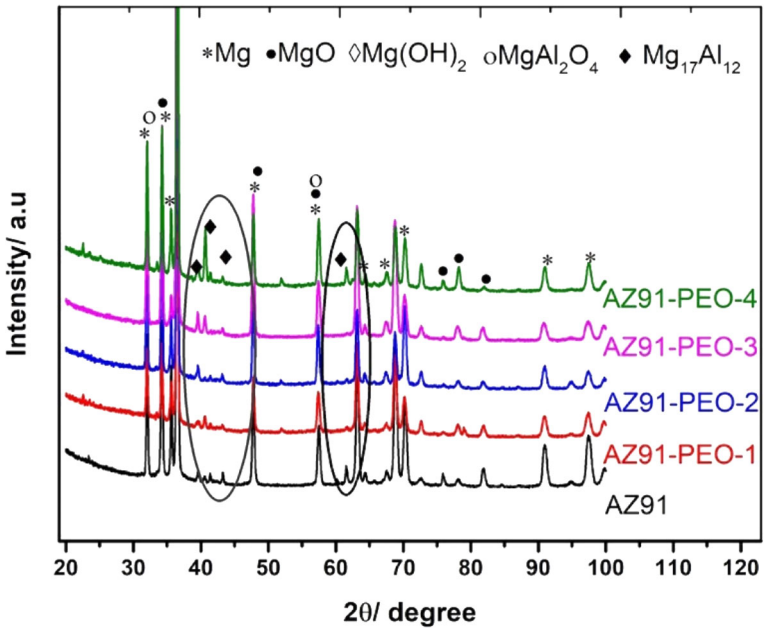

FIGURE 4 XRD patterns for as-received AZ91 and different PEO coated samples

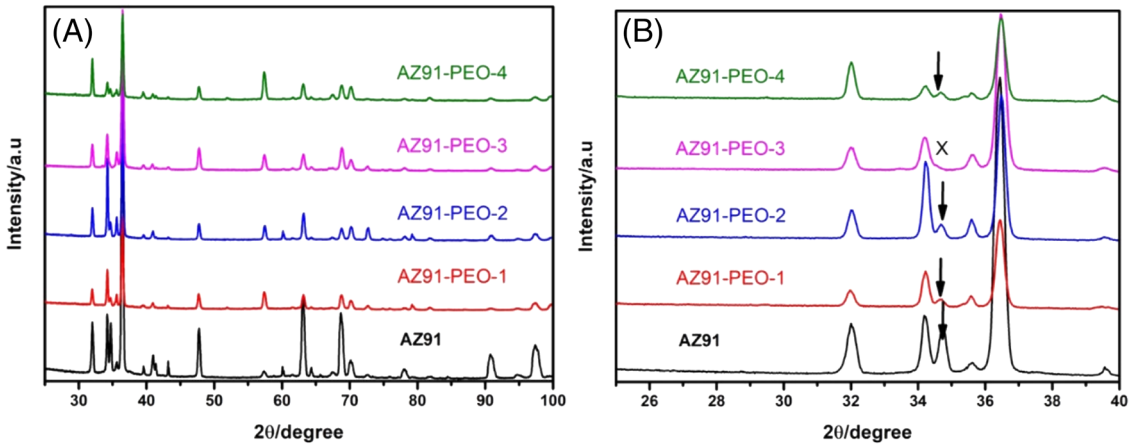

FIGURE 5 Full spectrum of XRD patterns obtained from as-received AZ91 and PEO coated samples after electrochemical corrosion test examined in aerated 0.5 M sodium chloride at 298 K (A), and a selected region from 26–40 2θ° to show the missing peak (B)

4.3 | Corrosion measurements

Figure 6 shows the free corrosion potential versus immersion time. All the PEO coatings showed a shift in potential toward the positive potentials, that is, more passive. Fluctuations in the potentials are appeared which can be attributed to the porosities on the coating surface. The as-received AZ91 sample shows no alternation in potential. The PEO-1 shows the highest peak, the widest range between the lowest and highest peaks, and most frequently peaks, while the PEO 2 and PEO 3 show less oscillation due to their small size pores, see Figure 1.

To investigate the corrosion performance of the coatings at sodium chloride [0.5 M], after reaching a stable free corrosion potential within 2 h of immersion, the EIS tests were applied on the samples. Figure 7, Nyquist plots, shows only one capacitive semicircle. The increase in its size indicates better corrosion protection of the PEO samples. For the low-frequency PEO sample, an inductive loop was not observed, which is an indication that the PEO process protects the dissolution and localized corrosion of the AZ91 alloy. While the inset part of the figure shows an inductive loop for the as-received alloy. The semicircle behavior is attributed to the charge transfer process whereas the inductive loop is

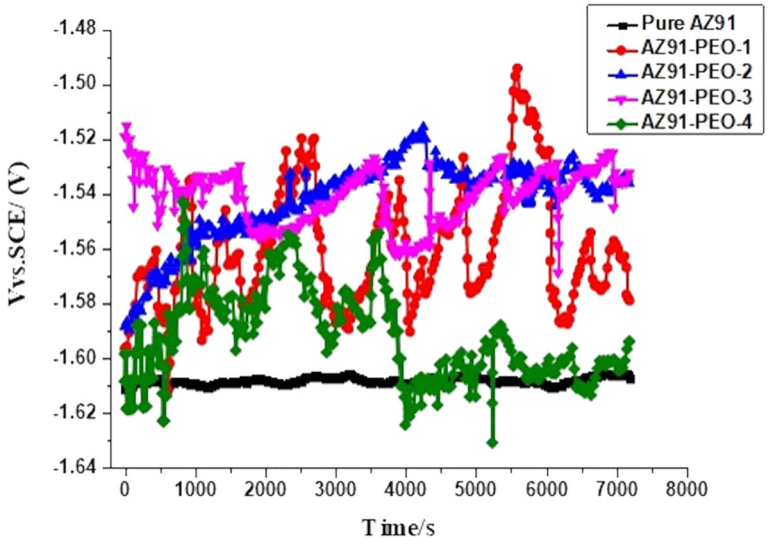

FIGURE 6 Open circuit potential versus time in the sodium chloride solution [0.5 M]

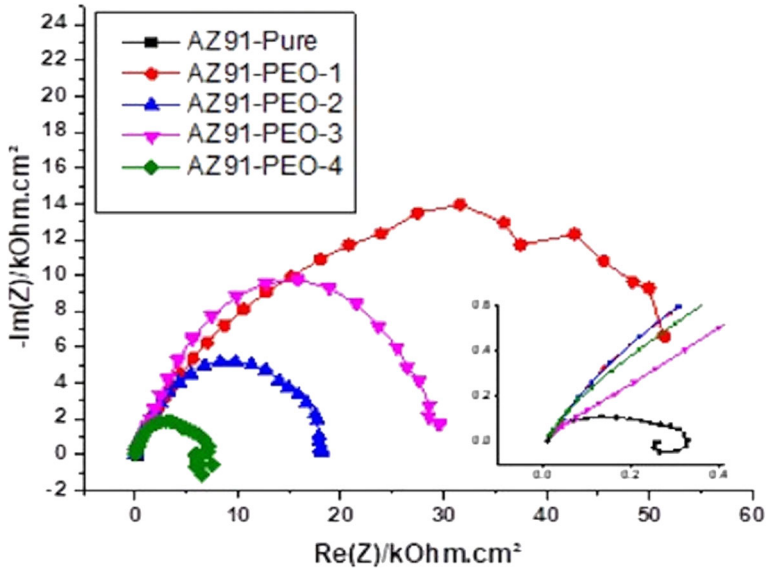

FIGURE 7 Nyquist plots of PEO coatings performance examined in 0.5 M of sodium chloride. The inset is the zoom-in impedance of the as-received AZ91

attributed to the dissolution of the substrate at the coating interface. Similar observations were reported by Reference 11,24,32.

Figure 8A, Bode plots, shows the enhancement of corrosion resistance after PEO treatment. The polarization resistance extrapolated at low frequency ($\log f = 0$) which was increased from 1×10^2 Ω to 1×10^4 Ω, indicating a better corrosion performance. Moreover, Figure 8B, shows that the phase angle of PEO coatings, for the high frequency, reached about −60°, indicating that PEO coatings provided better corrosion protection. In particular, the PEO-3 sample showed higher and wider capacitance like performance at intermediate and high frequency. This is attributed to the dense, that is, less porous, coatings obtained by applying higher pulsing frequency, see Figure 1.

Furthermore, the EIS data were modeled using EC labV10.37 software and the Randomize+ simplex method to examine the corrosion mechanism of the coatings at the electrode/electrolyte interface. The EIS data were fitted using two equivalent circuit models shown in Figure 9A,B for the as-received AZ91 and coated samples respectively. Table 2 lists the fitting results.

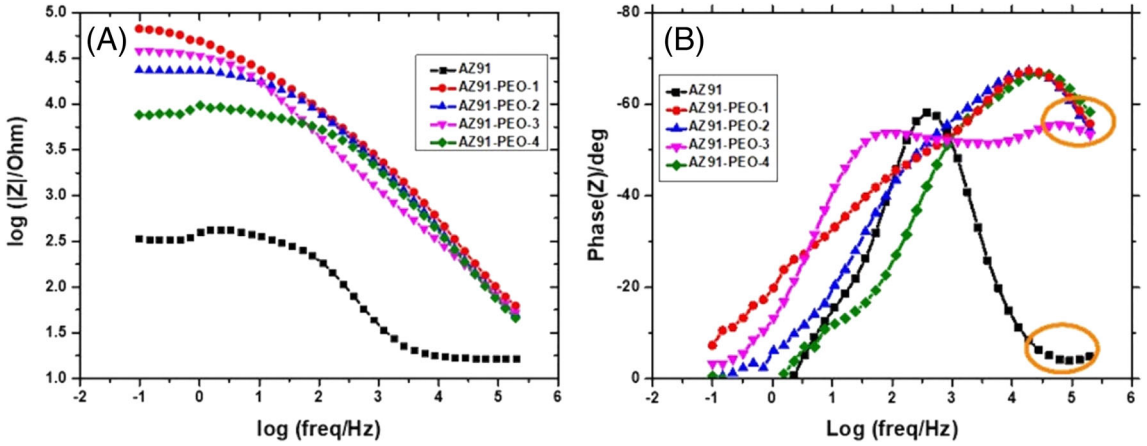

FIGURE 8 Bode plots (A) log |Z| versus log (freq/Hz), and (B) phase angle versus log (freq/Hz) of AZ91 and PEO coatings performance examined in 0.5 M of sodium chloride

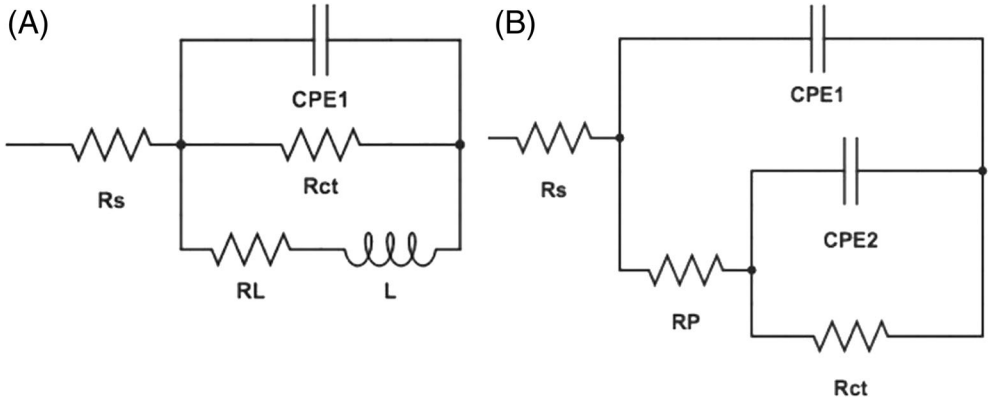

FIGURE 9 The equivalent circuits model for, (A) as-received AZ91, (B) PEO coated alloys

TABLE 2 The EIS fitting results of pure AZ91 alloy and different PEO coatings on AZ91 alloy examined in 0.5 M of sodium chloride

Samples	R_s (Ω cm^2)	CPE1 (Ω^{-1} s^n cm^{-2})	n_1	R_p (Ω cm^2)	CPE2 (Ω^{-1} s^n cm^{-2})	n_2	R_{ct} (Ω cm^2)	R_L (Ω cm^2)	L (H cm^{-2})	χ^2
AZ91	12.54	2.22×10^{-5}	0.86	NA	NA	NA	299	1135	481	0.124
AZ91-PEO-1	15.4	2.33×10^{-7}	0.83	1909	5.25×10^{-6}	0.48	6097	NA	NA	0.016
AZ91-PEO-2	12.49	3.80×10^{-7}	0.81	3125	2.19×10^{-6}	0.60	15,510	NA	NA	0.013
AZ91-PEO-3	6.06	1.89×10^{-6}	0.68	1375	1.02×10^{-6}	0.74	29,423	NA	NA	0.053
AZ91-PEO-4	4.9	6.69×10^{-6}	0.75	5484	7.17×10^{-6}	1	1320	NA	NA	0.177

Note: Two equivalent circuits were used.

The equivalent circuit model, for the as-received sample, displays five elements that is, R_s, CPE1, R_{ct}, R_L, and L for solution resistance, charge transfer resistance, constant phase element, pitting resistance, and inductance respectively. The sample showed small charge resistance and a short time constant of about 150 s. On the other hand, the EC model for the PEO coated samples, has no inductance and pitting corrosion resistance. The EC for PEO coatings displays two constant phase elements, CPE1and CPE2, and two resistances, which are R_p and R_{ct}, in addition to the solution resistance (R_s). At high frequency, a capacitive semicircle is dominated by CPE1 and polarization resistance (R_p) which are related

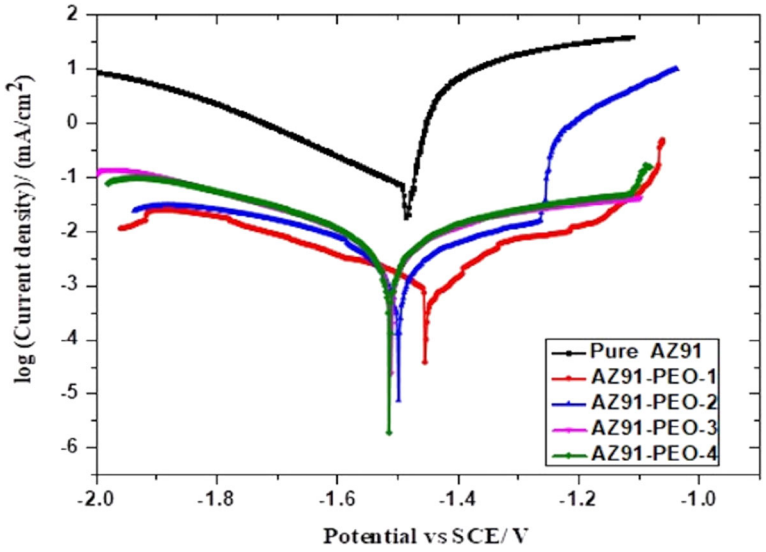

FIGURE 10 PDP curves of substrate and PEO coated samples carried out in 0.5 M sodium chloride

TABLE 3 Corrosion properties obtained from PDP curves

Samples	βa (mV dec^{-1})	$-\beta c$ (mV dec^{-1})	E_{corr} (V/SCE)	Breakdown potential (approx.) (V/SCE)	I_{corr} (μA cm^{-2})	Averaged I_{corr} (μA cm^{-2})	mmpy
AZ91	23.3	198	−1.479	−1.11	60.5	51.7	1.642
AZ91-PEO-1	85.7	215	−1.424	−1.22	0.739	0.77	0.023
AZ91-PEO 2	96.6	106	−1.495	−1.26	1.02	1.15	0.027
AZ91-PEO 3	141	116	−1.514	−1.161	2.2	0.77	0.060
AZ91-PEO 4	284	253	−1.510	−1.1	1.744	1.73	0.047

to the outer layer of the PEO coatings. At low frequency, CPE2 and charge transfer resistance (R_{ct}) are depicting the inner layer of the PEO coatings. A similar observation was obtained by Cue et al.[32] and Ling et al.[17]

Figure 10 shows PDP curves, which indicate a considerable improvement in the corrosion resistance of PEO coated samples. The current density of the PEO coated samples decrease by two orders of magnitudes. Also, the PEO samples show a passive range at high oxidative potentials. Table 3 shows the extrapolation results of the potentiodynamic curves, see Figure 10. Table 3 shows that the corrosion current density of the as-received alloy decreased from 60 μA cm^{-2} to around 1.7 μA cm^{-2} for the PEO samples. While the corrosion potentials of the as-received and PEO alloys were similar. The PEO-3 showed a wide range of passivation which complies with the results shown in Bode plots, also see Figure 8B. The as-received alloy-AZ91 did not show a clear breakdown potential at the studied potential ranges, however, we expect this may appear at potentials ranges around −1.11 V versus SCE. Although, the PEO samples show a passive range at high oxidative potentials, these passive films break down at potential ranges around 1.2 V versus SCE.

Corrosion resistances were extracted through applying linear polarization resistance (LPR) from a slope of the linear current-potential dependence at the free corrosion potential following Stern and Geary Equation 2[33]:

$$i_{corr} = \frac{1}{2.3}\frac{b_a\, b_c}{b_a + b_c}\left(\frac{di}{dE}\right)_{E_{corr}} = \frac{B}{R_p} \tag{2}$$

where B, i_{corr}, R_p are Tafel constant, corrosion current and polarization resistance respectively.

Figure 11 compares the results obtained by cyclic potentiodynamic curves with both the PDP and EIS results. The results show that current densities decreased for PEO coated samples. However, all PEO coated and the as-received AZ91

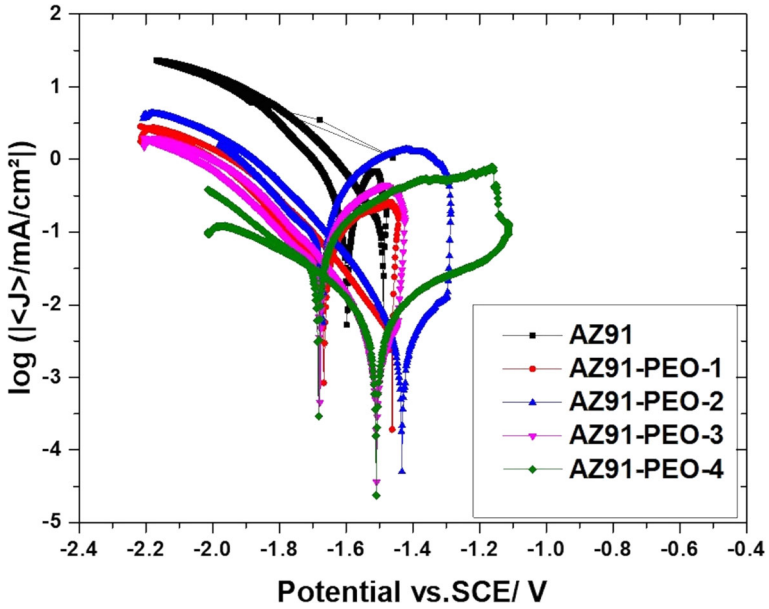

FIGURE 11 Cyclic PDP curves of coated AZ91 alloys in 0.5 M of NaCl solution

TABLE 4 Corrosion properties obtained from linear polarization resistance (LPR) curves

Samples	βa (mV dec^{-1})	$-\beta c$ (mV dec^{-1})	E_{corr} (V/SCE)	R_p Ohm cm^2	R_2	I_{corr} (μA cm^{-2})	mmpy
AZ91	23.3	198	−1.602	247	0.994	36.763	0.993
AZ91-PEO-1	85.7	215	−1.568	40, 238	0.994	0.662	0.017
AZ91-PEO 2	96.6	106	−1.535	18, 135	0.997	1.212	0.032
AZ91-PEO 3	141	116	−1.600	5861	0.994	4.720	0.127
AZ91-PEO 4	284	253	−1.584	8042	0.991	7.234	0.195

samples show positive hysteresis and negative re-passivation potential E_{rep}. This indicates that electrolytes were diffused into the micropores and instigated localized corrosion after a long time of immersion.

Table 4 shows the outcomes of the above tests and finding out the corrosion rate in mils per year (mmpy). The results show that all the PEO coated samples have a lower corrosion rate compared with the as-received AZ91 alloy. The highest mmpy value for the PEO samples is still lower than the as-received by at least 8 times.

5 | CONCLUSIONS

- PEO coating improves the corrosion resistance of magnesium alloy type AZ91.
- Bipolar current PEO processing mode with high frequency provides a smaller microprobe than unipolar.
- Bipolar waveform with higher frequencies provides a thinner, but denser, coating layer, consequently higher corrosion resistance.
- The AZ91-PEO3 displayed, smaller micropores, extended plateau (capacitor-like behavior) over middle, and high-frequency ranges.
- The mmpy values showed a large ratio, around 8:1, between the as-received to the PEO coated samples.
- Increasing duty cycle percentage for PEO process results in a compact thinner film with less porosity, consequently, better corrosion efficiency is obtained. However, the lower duty cycle percentage generates a bigger spark, leading to a porous coating which easily accelerates corrosion process.

ACKNOWLEDGMENT

The authors are grateful to King Abdulaziz City for Science and Technology (KACST) in the Kingdom of Saudi Arabia for supporting this project (Ref. no. 37502500) and for De Montfort University in the United Kingdom for scientific and technical supports.

CONFLICT OF INTEREST

The authors declare no potential conflict of interest.

AUTHOR CONTRIBUTIONS

Talal Aljohani: Conceptualization (lead); formal analysis (lead); investigation (lead); supervision (lead); validation (lead); writing – original draft (lead); writing – review and editing (equal). **Sami Aljadaan:** Conceptualization (supporting); data curation (equal); investigation (supporting). **Meteb Bin Rubayan:** Data curation (supporting); investigation (supporting); project administration (equal); software (equal). **Fuad Khoshnaw:** Data curation (equal); investigation (equal); writing – original draft (equal).

DATA AVAILABILITY STATEMENT

Data openly available in a public repository that issues datasets with DOIs

PEER REVIEW

The peer review history for this article is available at https://publons.com/publon/10.1002/eng2.12459.

ORCID

Talal A. Aljohani https://orcid.org/0000-0003-3530-8809
Fuad Khoshnaw https://orcid.org/0000-0002-4467-1944

REFERENCES

1. Kaseem M, Hussain T, Rehman ZU, Ko YG. Stabilization of AZ31 mg alloy in sea water via dual incorporation of MgO and WO3 during micro-arc oxidation. *J Alloys Compd*. 2021;853:157036. https://doi.org/10.1016/j.jallcom.2020.157036
2. Bordbar-Khiabani A, Yarmand B, Mozafari M. Effect of ZnO pore-sealing layer on anti-corrosion and in-vitro bioactivity behavior of plasma electrolytic oxidized AZ91 magnesium alloy. *Mater Lett*. 2020;258:126779. https://doi.org/10.1016/j.matlet.2019.126779
3. Heydarian A, Atapour M, Hakimizad A, Raeissi K. The effects of anodic amplitude and waveform of applied voltage on characterization and corrosion performance of the coatings grown by plasma electrolytic oxidation on AZ91 mg alloy from an aluminate bath. *Surf Coatings Technol*. 2020;383:125235. https://doi.org/10.1016/j.surfcoat.2019.125235
4. Mena-Morcillo E, Veleva L. Degradation of AZ31 and AZ91 magnesium alloys in different physiological media: effect of surface layer stability on electrochemical behaviour. *J Magnes Alloy*. 2020;8:667-675. https://doi.org/10.1016/j.jma.2020.02.014
5. Mordike BL, Ebert T. Magnesium properties—applications—potential. *Mater Sci Eng A*. 2001;302:37-45.
6. Witte F, Abeln I, Switzer E, Kaese V, Meyer-Lindenberg A, Windhagen H. Evaluation of the skin sensitizing potential of biodegradable magnesium alloys. *J Biomed Mater Res A*. 2008;86:1041-1047. https://doi.org/10.1002/jbm.a.31713
7. Witte F. The history of biodegradable magnesium implants: a review. *Acta Biomater*. 2010;6:1680-1692.
8. Pourbaix M, Zhang H, Pourbaix A. Presentation of an atlas of chemical and electrochemical equilibria in the presence of a gaseous phase. *Mater Sci Forum*. 1997;251–254:143-148. https://doi.org/10.4028/www.scientific.net/msf.251-254.143
9. Zhao L, Cui C, Wang Q, Bu S. Growth characteristics and corrosion resistance of micro-arc oxidation coating on pure magnesium for biomedical applications. *Corros Sci*. 2010;52:2228-2234. https://doi.org/10.1016/j.corsci.2010.03.008
10. Song Y, Dong K, Shan D, Han EH. Investigation of a novel self-sealing pore micro-arc oxidation film on AM60 magnesium alloy. *J Magnes Alloy*. 2013;1:82-87. https://doi.org/10.1016/j.jma.2013.02.009
11. Dong K, Song Y, Shan D, Han EH. Corrosion behavior of a self-sealing pore micro-arc oxidation film on AM60 magnesium alloy. *Corros Sci*. 2015;100:275-283. https://doi.org/10.1016/j.corsci.2015.08.004
12. Mathis A, Rocca E, Veys-Renaux D, Tardelli J. Electrochemical behaviour of titanium in KOH at high potential. *Electrochim Acta*. 2016;202:253-261. https://doi.org/10.1016/j.electacta.2015.11.027
13. Zhang XP, Zhao ZP, Wu FM, Wang YL, Wu J. Corrosion and wear resistance of AZ91D magnesium alloy with and without microarc oxidation coating in Hank's solution. *J Mater Sci*. 2007;42:8523-8528. https://doi.org/10.1007/s10853-007-1738-z
14. Cui LY, Fang XH, Cao W, et al. In vitro corrosion resistance of a layer-by-layer assembled DNA coating on magnesium alloy. *Appl Surf Sci*. 2018;457:49-58. https://doi.org/10.1016/j.apsusc.2018.06.240
15. Karpushenkov SA, Shchukin GL, Belanovich AL, Savenko VP, Kulak AI. Plasma electrolytic ceramic-like aluminum oxide coatings on iron. *J Appl Electrochem*. 2010;40:365-374. https://doi.org/10.1007/s10800-009-0005-1

16. Francis A, Virtanen S, Turhan MC, Boccaccini AR. Investigating the effect of salicylate salt in enhancing the corrosion resistance of AZ91 magnesium alloy for biomedical applications. *BioNanoMaterials*. 2015;2015:113–119. https://doi.org/10.1515/bnm-2015-0008
17. Liang J, Srinivasan PB, Blawert C, Dietzel W. Comparison of electrochemical corrosion behaviour of MgO and ZrO2 coatings on AM50 magnesium alloy formed by plasma electrolytic oxidation. *Corros Sci*. 2009;51:2483-2492. https://doi.org/10.1016/j.corsci.2009.06.034
18. Lu X, Blawert C, Zheludkevich ML, Kainer KU. Insights into plasma electrolytic oxidation treatment with particle addition. *Corros Sci*. 2015;101:201-207. https://doi.org/10.1016/j.corsci.2015.09.016
19. Yerokhin AL, Nie X, Leyland A, Matthews A, Dowey SJ. Plasma electrolysis for surface engineering. *Surf Coatings Technol*. 1999;122:73-93. https://doi.org/10.1016/S0257-8972(99)00441-7
20. Yin Z, He R, Chen Y, et al. Effects of surface micro–galvanic corrosion and corrosive film on the corrosion resistance of AZ91–xNd alloys. *Appl Surf Sci*. 2021;536:147761. https://doi.org/10.1016/j.apsusc.2020.147761
21. Rakoch AG, Monakhova EP, Khabibullina ZV, et al. Plasma electrolytic oxidation of AZ31 and AZ91 magnesium alloys: comparison of coatings formation mechanism. *J Magnes Alloy*. 2020;8:587-600. https://doi.org/10.1016/j.jma.2020.06.002
22. Barati Darband G, Aliofkhazraei M, Hamghalam P, Valizade N. Plasma electrolytic oxidation of magnesium and its alloys: mechanism, properties and applications. *J Magnes Alloy*. 2017;5:74-132.
23. Yang J, Lu X, Blawert C, Di S, Zheludkevich ML. Microstructure and corrosion behavior of Ca/P coatings prepared on magnesium by plasma electrolytic oxidation. *Surf Coatings Technol*. 2017;319:359-369. https://doi.org/10.1016/j.surfcoat.2017.04.001
24. Hussein RO, Northwood DO, Nie X. The effect of processing parameters and substrate composition on the corrosion resistance of plasma electrolytic oxidation (PEO) coated magnesium alloys. *Surf Coatings Technol*. 2013;237:357-368. https://doi.org/10.1016/j.surfcoat.2013.09.021
25. Lu X, Chen Y, Blawert C, et al. Influence of SiO2 particles on the corrosion and wear resistance of plasma electrolytic oxidation-coated AM50 mg alloy. *Coatings*. 2018;8:55–65. https://doi.org/10.3390/COATINGS8090306
26. Sreekanth D, Rameshbabu N, Venkateswarlu K. Effect of various additives on morphology and corrosion behavior of ceramic coatings developed on AZ31 magnesium alloy by plasma electrolytic oxidation. *Ceram Int*. 2012;38:4607-4615. https://doi.org/10.1016/j.ceramint.2012.02.040
27. Pezzato L, Coelho LB, Bertolini R, et al. Corrosion and mechanical properties of plasma electrolytic oxidation-coated AZ80 magnesium alloy. *Mater Corros*. 2019;70:2103-2112. https://doi.org/10.1002/maco.201910847
28. Cao FH, Cao JL, Zhang Z, Zhang JQ, Cao CN. Plasma electrolytic oxidation of AZ91D magnesium alloy with different additives and its corrosion behavior. *Mater Corros*. 2007;58:696-703. https://doi.org/10.1002/maco.200704050
29. Ghasemi A, Raja VS, Blawert C, Dietzel W, Kainer KU. Study of the structure and corrosion behavior of PEO coatings on AM50 magnesium alloy by electrochemical impedance spectroscopy. *Surf Coatings Technol*. 2008;202:3513-3518. https://doi.org/10.1016/j.surfcoat.2007.12.033
30. Duan H, Yan C, Wang F. Growth process of plasma electrolytic oxidation films formed on magnesium alloy AZ91D in silicate solution. *Electrochim Acta*. 2007;52:5002-5009. https://doi.org/10.1016/j.electacta.2007.02.021
31. Esmaily M, Mortazavi N, Svensson JE, et al. Atmospheric corrosion of mg alloy AZ91D fabricated by a semi-solid casting technique: the influence of microstructure. *J Electrochem Soc*. 2015;162:C311-C321. https://doi.org/10.1149/2.0341507jes
32. Cui LY, Gao SD, Li PP, et al. Corrosion resistance of a self-healing micro-arc oxidation/polymethyltrimethoxysilane composite coating on magnesium alloy AZ31. *Corros Sci*. 2017;118:84-95. https://doi.org/10.1016/j.corsci.2017.01.025
33. Stern M. Electrochemical polarization. *J Electrochem Soc*. 1957;104:559. https://doi.org/10.1149/1.2428653

How to cite this article: Aljohani TA, Aljadaan S, Bin Rubayan MT, Khoshnaw F. Impact of processing parameters in plasma electrolytic oxidation on corrosion resistance of magnesium alloy type AZ91. *Engineering Reports*. 2021;e12459. doi: 10.1002/eng2.12459